Atmos. Chem. Phys. Discuss., 11, 2317–2354, 2011
www.atmos-chem-phys-discuss.net/11/2317/2011/
doi:10.5194/acpd-11-2317-2011

Atmospheric Chemistry and Physics Discussions

An important fingerprint of wildfires on the European aerosol load

F. Barnaba[1], **F. Angelini**[1], **G. Curci**[2], **and G. P. Gobbi**[1]

[1]Istituto di Scienze dell'Atmosfera e del Clima, Consiglio Nazionale delle Ricerche (ISAC-CNR), Roma, Italy
[2]CETEMPS-Dipartimento di Fisica, Università degli Studi dell'Aquila, L'Aquila, Italy

Received: 7 December 2010 – Accepted: 11 January 2011 – Published: 21 January 2011

Correspondence to: F. Barnaba (f.barnaba@isac.cnr.it)

Published by Copernicus Publications on behalf of the European Geosciences Union.

Abstract

Wildland fires represent the major source of accumulation mode aerosol (i.e., atmospheric particles with diameters <1 µm). The largest part of these fires occurs in Africa, Asia and South America, but a not negligible fraction also occurs in Eastern Europe and former USSR countries, particularly in the Russian Federation, Ukraine and Kazakhstan. Apart for exceptional cases as the Russian fires of summer 2010, routine agricultural fires in Eastern Europe and Russia have been recently shown to play a crucial role in the composition of the Arctic atmosphere. However, an evaluation of the impact of these fires over Europe is currently not available. The assessment of the relative contribution of fires to the European aerosol burden is hampered by the complex mixing of natural and anthropogenic particle types over the continent. In this study we use long term (2002–2007) satellite-based fires and aerosol data coupled to atmospheric transport modelling to attempt unravelling the wildfires contribution to the European aerosol optical thickness (AOT). Based on this dataset, we provide evidence that fires-related aerosol emissions play a major role in shaping the AOT yearly cycle at the continental scale. In general, the regions most impacted by wildfires emissions and/or transport are Eastern and Central Europe as well as Scandinavia. Conversely, a minor impact is found in Western Europe and Western Mediterranean. We estimate that in spring 5 to 35% of the European fine fraction AOT (FFAOT, i.e., the AOT due to accumulation mode particles) is attributable to wildland fires. The calculated impact maximizes in April (20–35%) in Eastern and Central Europe as well as in Scandinavia and in the Central Mediterranean. An important contribution of wildfires to FFAOT is also found in summer over most of the continent, particularly in August over Eastern Europe (28%) and the Mediterranean regions, from Turkey (34%) to the Western Mediterranean (25%). This unveiled, fires-related, continent-wide haze is expected to play a not negligible role on the European radiation budget, and possibly, on the European air quality, therefore representing a clear target for mitigation.

ACPD
11, 2317–2354, 2011

1 Introduction

The uncontrolled use of fire for clearing forest and woodland for agriculture is estimated to account for up to 90% of world's wildland fires (FAO, 2009). In the European area, the majority of the wildland fires occurs in the cropland-dominated areas of Eastern Europe and European Russia, with a major role played by former USSR countries as Ukraine, Kazakhstan and Russian Federation. In these regions, a remarkable 50–70% of all fires detected from satellite in 2001–2003 were cropland burning (Koronzti et al., 2006). In the Russian Federation, about 90% of fires in the period 2002–2005 were started by people (Mollicone et al., 2006).

In terms of emissions, biomass burning during wildland fires is an important source of trace gases and one of the largest global contributors to accumulation mode aerosols, i.e., atmospheric particles with diameters <1 µm (e.g., Kasischke and Penner, 2004; Reid et al., 2005a). These emissions can be transported over long distances, leading to regionally elevated aerosol loadings (e.g., Damoah et al., 2004; McMeeking et al., 2006; Hodzic et al., 2007).

The major role agricultural fires in Eastern Europe and Russia play in the composition of the Arctic atmosphere has been recently highlighted (e.g., Generoso et al., 2007; Stohl, 2007; Warneke et al., 2010). Several studies also investigated properties and impacts of biomass burning events on aerosol properties at different European sites/regions (e.g., Formenti et al., 2002; Balis et al., 2003; Pace et al., 2005; Muller et al., 2005; Niemi et al., 2005; Arola et al., 2007; Witham and Manning, 2007; Hodzic et al., 2007; Sciare et al., 2008; Amiridis et al., 2009; Saarnio et al., 2010). However, being fragmented in space and time, this broad literature does not allow to draw a more general picture of the impact of fires on the aerosol loads at the continental scale. Still, meteorological fields over the continent are often favourable to easterly transports, particularly in spring, when agricultural fire activity is maximum (the dispersion of the Chernobyl radioactive plume towards Central Europe in April 1986 testifies the importance of such advections).

ACPD
11, 2317–2354, 2011

Current capabilities of global or regional chemistry-transport models to include accurately quantified fires emissions and reproduce some relevant aerosol properties are also affected by large uncertainties (e.g., Kasischke and Penner, 2004; Wiedinmyer et al., 2006; Langmann et al., 2009; Menut and Bessagner, 2010). Thus a reliable model-based assessment of the impact of fires on the European aerosol load is also lacking.

In this study we formulate the hypothesis and provide observational evidences that, over the whole European continent, wildland fires play a major role in modulating the yearly cycle of the aerosol load, and particularly its fine mode fraction. The term wildland fires is employed here to denote open fires of various vegetation (e.g., forests, grasslands, agricultural residues) and peat that are set by humans or occur naturally (e.g., by lightening), the latter representing an almost negligible portion of the total.

In particular, we focus on the impact of wildfires on the European "aerosol optical thickness" (AOT), this being the aerosol optical parameter at the basis of aerosol radiative forcing computations, i.e., at the basis of aerosol climatic impact evaluations (e.g., Tegen et al., 2000; Marmer et al., 2007).

Over Europe and the Mediterranean, the AOT is typically build up by a complex mixture of different components of both natural and anthropogenic origin. Marine particles from the surroundings seas and desert dust advected from the nearby Sahara desert mix, in variable proportions, with local and/or long-range transported pollution produced by human activities (e.g., Barnaba and Gobbi, 2004). In this region, the AOT yearly cycle typically shows a winter minimum and a spring/summer maximum (e.g., Yu et al., 2003; Edwards et al., 2004; Papadimas et al., 2008; Chubarova, 2009), with some interannual and spatial variability. This annual AOT behaviour is mainly driven by in-phase annual cycles of major aerosol-source factors (e.g., radiation, which favours secondary aerosol formation, and convection, which facilitates particles and gases injection and mixing into the atmosphere), and opposite cycles of major aerosol removal agents as wind speed and precipitation (e.g., Koelemeijer et al., 2006; Mehta and Yang, 2008; Papadimas et al., 2008; Chubarova, 2009).

ACPD
11, 2317–2354, 2011

Deviations from a "regular", sinusoidal-like AOT cycle have been however observed in Europe. Some of these deviations are attributable to the transport of Saharan dust advections towards the Mediterranean and Europe, an important season dependent phenomenon which typically maximizes in spring/summer and minimizes in winter (e.g., Moulin et al., 1998; Barnaba and Gobbi, 2004; Papayannis et al., 2008). However, other, systematic seasonal increases of AOT in spring and summer have been observed which cannot be attributed, or uniquely attributed, to Saharan dust transport since mainly associated to fine particulate (e.g., Aculinin et al., 2004; Chubarova, 2009; Sicard et al., 2011). Vegetation fires in Eastern Europe or in the Mediterranean countries have been shown to enhance the local aerosol load, particularly in the hottest periods/countries, when relatively small-scale, human-initiated fires often quickly develop into uncontrolled widespread fires (e.g, Hodzic et al., 2007; Sciare et al., 2008; Amiridis et al., 2009).

This study unveils the impact of these wildfires is almost ubiquitous over the European continent and points out the currently underrated role of agricultural burning in modulating the AOT yearly cycle. In particular, using long term (2002–2007) satellite aerosol and fires observations coupled to atmospheric transport modelling, we provide monthly-resolved quantitative estimates of the wildfires contribution to the fine fraction AOT in the different European regions.

2 Methods

This study focuses on the 6-year period 2002–2007 and employs 1) Aerosol Optical Thickness (AOT) data from the MISR sensor on board the NASA-Terra platform (e.g., Martonchik et al., 2009; Kahn et al., 2010), 2) fires data (both Fire Counts, FC, and Fire Radiative Power, FRP, data) from the MODIS sensor on board the same NASA-Terra platform (e.g., Giglio et al., 2003, 2006), 3) forward trajectories computed by means of the NOAA-HYSPLIT Lagrangian integrated trajectory model (Draxler and Hess, 1998).

ACPD
11, 2317–2354, 2011

To investigate the aerosol variability during the year, monthly statistics of significant parameters were considered and further averaged over seven selected European target regions covering most of the continent. These regions (Fig. 1) are: Scandinavia (5° to 28° E; 56° to 64° N, cyan shaded area), Western Europe (–11° to –7° E; 46° to 56° N, magenta shaded area), Central Europe (7° to 25° E; 46° to 56° N, green shaded area), Eastern Europe (25° to 42° E; 46° to 56° N, reddish shaded area), Western Mediterranean (–11° to –7° E; 36° to 46° N, orange shaded area), Central Mediterranean (7° to 25° E, 36° to 46° N, bluish shaded area) and Turkey (25° to 42° E; 36° to 46° N, gray shaded area).

Details on the datasets and data processing are described hereafter.

2.1 MISR AOT data

The MISR instrument (Diner et al., 1998) infers AOT by using observations of nine cameras pointing at different angles and separates aerosol from land scattering based on the angular distribution of the up-welling radiance phase function. Details on the MISR aerosol retrieval can be found in Martonchik et al. (2009). The quality of the MISR aerosol products has been carefully evaluated by Kahn et al. (2010) through the comparison with relevant aerosol data from the worldwide AERONET sunphotometer network (Holben et al., 1998). Results indicate 70% to 75% of MISR AOT retrievals to fall within 0.05 or 20%×AOT of the paired validation data from AERONET, and 50% to 55% to fall within 0.03 or 10%×AERONET AOT, except at sites where dust, or mixed dust and smoke, are commonly found.

In this study we employ monthly mean Level 3, 0.5°×0.5° resolution MISR aerosol data (MIL3MAE dataset). We use the latest released (version 31) AOT dataset (at 555 nm) and the relevant AOT due to the aerosol finest fraction (i.e., AOT due to particles having radius smaller than 0.35 µm, hereafter referred to as FFAOT). The AOT dataset is a MISR Validated Stage 3 product (i.e., uncertainties are estimated from independent measurements representing global conditions) whereas the MISR particle

ACPD
11, 2317–2354, 2011

size fractional AOT amounts are Validated Stage 2 products (i.e., uncertainties are estimated from more widely distributed independent measurements).

2.2 MODIS fires data

We use monthly mean fires counts (FC, counts/m^2/day) and fire radiative power (FRP, MW or Mj s^{-1}) data from MODIS-Terra. The fire detection by satellite is performed exploiting their strong emissions of mid-infrared radiation. MODIS fires retrieval uses a contextual algorithm based on the brightness temperature derived from the 4 µm and 11 µm channels (Giglio et al., 2003). Detailed information about the MODIS fire products can be found in Justice et al. (2006).

The FC dataset used in this study is the MODIS-Terra overpass corrected fire pixel count product available through the NASA Earth Observation (NEO) portal (http://neo.sci.gsfc.nasa.gov). It is a gridded statistical summary of fire pixel information intended for use in regional and global modelling with a spatial resolution of 0.5° for time periods of one calendar month (Justice et al., 2006). To provide a view of the typical spatial-temporal variability of fire counts in Europe, the monthly mean number of fires computed over the whole period addressed here (2002–2007) is shown as coloured circles in Fig. 1.

Fires release heat energy which propagates in space and facilitates fire detection by remote sensing. Satellite observations actually measure the rate at which energy is emitted by a fire during the combustion, i.e., the Fire Radiative Power, FRP (e.g., Kaufman et al., 1998; Giglio et al., 2003; Wooster et al., 2005). This can serve as an indicator of the rate of aerosols (and gases) released (e.g., Kaufmann et al., 1998). FRP estimated accuracy from MODIS is of about 15% (Wooster et al., 2005). In this study we use MODIS-Terra monthly FRP data at 1° by 1° resolution (MODIS Active Fire Product MOD14CM1, version V005) available through the Giovanni web-based application (http://disc.sci.gsfc.nasa.gov/giovanni), developed by the NASA Goddard Earth Sciences Data and Information Services Center (GES DISC) (Acker and Leptoukh, 2007).

ACPD
11, 2317–2354, 2011

2.3 Forward trajectory computations

We use the NOAA-HYSPLIT Lagrangian integrated trajectory model (http://ready.arl.noaa.gov) to compute 10-day forward trajectories originating from fires detected in the domain from −20° to 70° E and from 20° to 70° N (dashed line-delimited area in Fig. 1). Horizontal resolution of trajectory computations was set at 2.5°, chosen as a compromise between good spatial resolution and acceptable computing time. A minimum fire count threshold of 25 fire counts/1000 km^2/day was set to start a trajectory computation (which corresponds to an average of 1 fire count/1000 km^2/day in the 25, 0.5° by 0.5° cells that compose the 2.5° by 2.5° grid box). One trajectory per day was computed for the whole 2002-2007 period, starting at 10:30 LT (i.e., close to the Terra overpass time). The starting altitude of trajectories was set at 500 m agl. Note that sensitivity tests showed minor changes in the results for starting altitudes within the first 1000 m, i.e., within the expected planetary boundary layer. Overall, a total of about 360000 forward trajectories is included in this study.

2.3.1 Coupling fires data and forward trajectory computations

With the aim of evaluating the contribution of fires to the AOT, a specific quantity has been defined and used as a proxy for the coupling of fire emissions with atmospheric dispersion capabilities. This quantity, in the following referred to as Fire Weighted Trajectory Density (FWTD), has been derived following the methodology detailed below and illustrated in Fig. 2.

To match the horizontal resolution of the forward trajectory computations, we first re-mapped the monthly fields of both the Fire Radiative Power and Fire Counts on a 2.5° by 2.5° grid. Each cell n of the European domain considered (area delimited by the dashed line in Fig. 1) is thus associated to a monthly mean FRP (and FC) value, FRP_n (and FC_n). For each day of the month (starting month, sm), a 10-day forward trajectory T_n originating at the centre of cell n is computed with hourly resolution time step (provided that FC_n>25 fire count/1000 km^2/day). For a given cell q along the T_n

ACPD
11, 2317–2354, 2011

path, we compute the contribution of T_n to q as:

$$\mathrm{FWTD}(\mathrm{am},\mathrm{day},n,q) = \mathrm{FRP}_n(\mathrm{sm}) \sum_{t_h} \exp(-t_h/\tau) \quad (1)$$

where am is the arrival month (which, depending on the starting day, may or not coincide with the starting month, sm), t_h is the time of travel (in hours) from the starting cell n to cell q. The sum over t_h accounts for the fact that a single T_n can spend more time steps over cell q. The exponential decay is used to take into account the typical lifetime of aerosol in the troposphere (e.g., Rangarajan, 1992; Ahmed et al., 2004; Papastefanou, 2006). In particular, a time constant τ=5 days (i.e., 120 h) has been set which also allows to avoid sharp transitions at the end of the 10-day forward trajectories (after 10 days of travel the FRP_n corrected for the exponential decay is about 10% of the original value).

Integrating the contribution to cell q of each cell n (and thus trajectory T_n) of the domain, we get:

$$\mathrm{FWTD}(\mathrm{am},\mathrm{day},q) = \sum_{n=1}^{N} \mathrm{FRP}_n(\mathrm{sm}) \sum_{t_h} \exp(-t_h/\tau) \quad (2)$$

Considering all the days in the month we obtain, for each cell q:

$$\mathrm{FWTD}(\mathrm{am},q) = \sum_{\mathrm{day}=1}^{D} \sum_{n=1}^{N} \mathrm{FRP}_n(\mathrm{sm}) \sum_{t_h} \exp(-t_h/\tau) \quad (3)$$

Examples of the so derived FWTD field over Europe for the months of April and July (average of the period 2002–2007) are shown in Fig. 3a and b, respectively (the complete set of the 12 months FWTD-field is given in a supplementary Fig. S1). Figure 3a clearly shows the April fires (mostly detected over Eastern Europe/Ukraine as shown in Fig. 1) to impact the whole continent, and particularly the north eastern sector. In

ACPD
11, 2317–2354, 2011

July (Fig. 3b), the contribution of fires from the Mediterranean countries (Spain, Italy, Greece) and the North African regions is also well visible.

The FWTD(am,q) field has then been averaged over the seven selected European target regions (TR), obtaining monthly and regionally resolved values:

$$\mathrm{FWTD} = \frac{1}{Q} \sum_{q \in TR} \sum_{\mathrm{day}=1}^{D} \sum_{n=1}^{N} \mathrm{FRP}_n(\mathrm{sm}) \sum_{t_h} \exp(-t_h/\tau) \quad (4)$$

where Q is the total number of cells belonging to TR (the dependence of FWTD on the month, am, and target region has been omitted for brevity, as will be done in the following). The so derived monthly and regionally resolved quantities will be presented and discussed in the next sections.

3 Results

For each year of the 2002–2007 period, the monthly AOT and FFAOT datasets were both averaged regionally over the seven addressed European regions of Fig. 1. In Fig. 4 we show the monthly mean AOT and FFAOT (squares and triangles, respectively) for the whole period 2002–2007 for each target region (panels a to g). The figure confirms the expected maximum aerosol load in spring/summer and minimum in winter and further shows that AOT generally follows a bimodal yearly cycle with maxima in April and July. This bimodality, particularly marked in the Central and Eastern European regions and less detectable in the Western ones, is even more clearly evident in the fine fraction AOT than in the total aerosol optical thickness. FFAOT over Europe is found to account for approximately 35% to 70% of the total AOT, with the maximum values and relative contributions in Eastern Europe and the minima in Turkey and Western Mediterranean, i.e., in the regions with the highest expected load of soil-derived (desert and/or local) coarse particles.

The interannual variability associated to both the AOT and FFAOT monthly means (shaded area corresponding to ±1 s.d. in Fig. 4) is also interesting. In fact, Fig. 4

ACPD
11, 2317–2354, 2011

shows this variability to display two minima, the first in the winter months and the other at mid-year (typically in May-June), when the local minimum between the two bimodal peaks occurs. This suggests the two maxima to be related to phenomena having a non negligible inter-annual variability. On the other hand this variability cannot be attributed, or at least cannot be uniquely attributed, to desert dust advection as (1) it shows the same yearly pattern in both AOT and FFAOT and (2) desert dust advection towards Europe and the Mediterranean is maximum in spring and summer (e.g., Moulin et al., 1998; Barnaba and Gobbi, 2004), a fact that would not agree with the observed AOT decrease in June.

The monthly and regionally averaged Fire Weighted Trajectory Density (FWTD) values, obtained as described in Sect. 2.3, are shown in Fig. 4 (gray diamonds, right axis) for direct comparison with the AOT cycles. We find a clear bimodality in the FWTDs, with a timing very similar to that of AOT and FFAOT, particularly evident in the Central and Eastern Europe regions. Also note that, as for the AOT cases, the variability associated to the FWTD minimizes in winter and in the mid-year minimum (May–June) between the two maxima. The FWTD seasonality is mainly driven by the characteristic bimodality of the agricultural fire activity in Europe, with two maxima in spring and summer corresponding to the planting and harvesting periods, respectively (Korontzi et al., 2006). In summer, an additional contribution from natural and/or human initiated fires invigorated by dryness and hot temperatures is also expected to contribute to the FWTD values observed, especially in the southernmost European regions.

Overall, a very good correlation ($R \geq 0.8$) between FFAOT and FWTD values is found in each region, confirming the hypothesis that a strong link between the fine aerosol optical thickness observed and the fire source exists.

To investigate the role of Mediterranean and Eastern Europe fires in generating the results of Fig. 4, we further divided the whole origin region considered for the FWTD computations (dashed area in Fig. 1) into four quadrants (Q1, Q2, Q3, Q4 in Fig. 1). The absolute and relative contributions from these quadrants to the total FWTD values are shown in Fig. 5 (area graphs and histograms, respectively). Figure 5 shows fires in

ACPD
11, 2317–2354, 2011

the southwest quadrant Q1 (which includes the Southern European states of Portugal, Spain, Italy, Greece, Slovenia and the others former Yugoslavia countries as well as Northern Africa) to have an important impact on the total FWTD only in two of the seven target European regions considered, namely Western Med and Central Med. In fact, in these two regions Q1 fires account for more than 45–50% of the FWTD during all winter, summer and autumn months. Only in the spring period this contribution decreases to about 40% and 25% in Western and Central Med, respectively, due to the increasing relative weight of Q3 fires. In the other target regions, the portion of FWTD due to fires originating in Q1 maximizes in summer, but its relative contribution keeps lower than 20%. Conversely, fires originating in the NE European quadrant Q3 (which includes Ukraine, Moldova, Belarus, Russia, Kazakhstan) are found to impact the whole continent during most of the year, and particularly in spring (see also Fig. 3a). In April, the minimum contribution of Q3 fires to the total FWTD is about 45% (in Western Europe and Western Med) while high contributions are obtained for Central Med and Central Europe (about 60%), Turkey and Scandinavia (about 70%) and Eastern Europe (85%). A minor role is played by Q2 and Q4 fires, whose effects are found to be mostly local (see for example the Q2 fires impact on the Turkey FWTD values, Fig. 5g).

This analysis suggests a larger impact of spring agricultural fires on the continental AOT with respect to the summer ones, which are mostly associated to the burning of other type of vegetation (e.g., forests). The more marked fingerprint of agricultural fires in spring with respect to summer was also reported by Sciare et al. (2008) based on long term in situ aerosol measurements performed in Creete (Greece). In particular, rather low OC/EC ratios were observed in spring compared to summer which are more compatible to agricultural waste burning (e.g., Andreae and Merlet, 2001; Hays et al., 2005). The reason for higher enhancement ratios of elemental carbon in the agricultural fire plumes with respect to forest fire plumes reflects the fact that agricultural fires burn at lower temperatures and tend to smoulder, emitting higher concentrations of products from incomplete carbon combustion. From an optical point of view, enrichment of elemental carbon translates into enhanced aerosol absorption, thus enhanced

ACPD
11, 2317–2354, 2011

aerosol extinction, and thus enhanced AOT.

3.1 Estimating wildfires contribution to the fine fraction AOT

In this study we assume that the impact of wildfires on the optical aerosol load is limited to the fine fraction AOT (FFAOT). In fact, being mainly the result of condensation/coalescence processes, biomass burning particles are predominantly found in this accumulation mode size range (e.g., Reid, 2005a; Janhall et al., 2010). This assumption also allows minimizing, although not eliminate, in our analysis possible "disturbances" by mineral dust or marine aerosol particles contribution to the AOT, mainly expected in the coarse aerosol fraction (e.g., d'Almeida et al., 1991).

Two approaches have been used to estimate the mean contribution of wildfires to the FFAOT over Europe. The first one is based on the measurement-derived FFAOT data while the second one also includes the FWTD computations formulated here (see Sect. 2.3).

In the first case (indicated with the subscript 1) we assume the monthly mean FFAOT values in each region to be the result of the contribution of a regional background ($FFAOT_{RB}$) plus that of wildfires ($FFAOT_{WF}$), i.e., for each month, m_i, it is:

$$FFAOT(m_i) = FFAOT_{RB}(m_i) + FFAOT_{WF,1}(m_i) \quad (5)$$

We then assume the regional background FFAOT to follow a sinusoidal behaviour during the year, as supported by climatological evidences in mostly unperturbed regions (e.g., Yu et al., 2003). For each region, the $FFAOT_{RB}$ is thus obtained fitting with a sine function the measurements-based FFAOT values of all those months in which, based on the FWTD computations, the expected wildfires contribution is negligible (January, February, November, December) or minimum (May or June, depending on the region). The $FFAOT_{RB}$ curves obtained are shown in Fig. 6 (thin black lines) together with the original MISR FFAOT dataset from which these were computed (continuous colour lines).

ACPD
11, 2317–2354, 2011

The derived $FFAOT_{WF,1}$ values (Eq. 5) are shown as coloured triangles in Fig. 6, the colour indicating the relative (%) contribution of $FFAOT_{WF,1}$ to the total FFAOT.

In the second case (indicated with subscript 2), we assume the FWTD obtained in each region to be proportional to the wildfires-related FFAOT, through a region-dependent conversion factor, CF, i.e.:

$$FFAOT_{WF,2}(m_i) = CF \times FWTD(m_i) \quad (6)$$

The conversion factor is computed only considering those months, m_j, with a not negligible wildfires contribution, i.e., those months not used to compute the sinusoidal fit describing $FFAOT_{RB}$. In particular, for each region, it is:

$$CF = \text{mean}[(FFAOT(m_j) - FFAOT_{RB}(m_j))/FWTD(m_j)] \quad (7)$$

The CF values obtained in the seven European target regions addressed are summarized in Table 1.

The derived $FFAOT_{WF,2}$ values (Eq. 6) are shown as coloured squares in Fig. 6, the colour indicating the relative (%) contribution of $FFAOT_{WF,2}$ to the total FFAOT.

Finally, for direct comparison with the MISR measured one, the FWTD-based FFAOT is also reconstructed as:

$$FFAOT_{FWTD}(m_i) = FFAOT_{WF,2}(m_i) + FFAOT_{RB}(m_i) \quad (8)$$

This is reported as dash-dotted lines in Fig. 6. Figure 6 shows the two estimates to follow very similar yearly patterns and to have rather close absolute value, except for few cases (e.g., March values in Western Europe). We then use their average value, $FFAOT_{WF\_mean}$ (Table 2), as a final indication of the estimated regionally and monthly average contribution of wildfires to the total FFAOT measured by MISR over Europe. This analysis indicates that, in spring and summer, 10 to 30% of the fine aerosol optical thickness in Europe is related to wildfires emissions (Table 2). In April the maximum impact of wildfires on the fine fraction AOT (relative weight of 20–35%) is found in Central and Eastern Europe, in Scandinavia and in the Central Mediterranean, while in August

ACPD
11, 2317–2354, 2011

the wildfires contribution to the FFAOT overcomes 25% in all the addressed regions but Western Europe. In general, the regions less affected by wildfires emissions and/or transport appear to be the western ones (Western Europe and Western Med) while, as expected, the most impacted are Eastern and Central Europe as well as Scandinavia.

Major uncertainties in Table 2 estimates (i.e., maximum standard deviations related to maximum difference between the corresponding $FFAOT_{WF,1}$ and $FFAOT_{WF,2}$ values) are found for the months of May and/or June. This is likely because in May or June, depending on the region, the $FFAOT_{WF,1}$ contributions have been necessarily forced to be zero by the sinusoidal fit used, whereas a minimum but not null contribution (as the one derived from the FWTD, i.e., $FFAOT_{WF,2}$), is probably much more realistic.

It is also worth commenting on the good agreement among the CF values obtained for the different regions (Table 1), giving robustness to the FWTD-to-FFAOT conversion approach adopted. The only exception is found for the Scandinavia value (more than twice the others CFs), also associated to a rather large variability. The higher CF derived for this region to match the observed FFAOT values suggests that the FWTD computations in this region are probably underestimated. We speculate this is likely due to an additional contribution of fires from regions east of 70° E, which are not accounted for in our study (see Sect. 2.3). In fact, similarly to the Arctic case (Sthol, 2007), Siberian/Asian fires might still have a significant impact at the European northernmost latitudes, particularly in spring, when temperatures are still low and quasi-isentropic transport of cold air from such regions is a potential pathway into the lower troposphere. These fires are conversely expected to have minor impacts over most of continental and Mediterranean Europe.

3.2 On the possible contribution from intercontinental transport

One question that may arise is whether, and to which extent, the FFAOT pattern observed over Europe is also influenced by intercontinental transport of pollution from other areas. In particular, given the general westerly circulation of the Northern Hemisphere, transport from North America might provide a not negligible contribution to the

ACPD
11, 2317–2354, 2011

European AOT (and mainly FFAOT) levels (e.g., Penkett et al., 2003; Huntrieser et al., 2005; Li et al., 2005), which, in principle, could bias our results. To check this possibility we further selected nine "control regions" over the Atlantic Ocean, off the European coasts (labelled A to I in Fig. 1), and applied our analysis also to these. Boundaries of the control regions were chosen in order to investigate both latitudinal and longitudinal AOT gradients from Europe as a function of the prevailing atmospheric circulation.

Yearly cycles of the MISR FFAOT in the nine control regions are reported in Fig. 7 (thick gray lines). As expected, FWTD values computed for these regions are negligible (at least two order of magnitude lower than those derived in the seven European target regions and shown in Fig. 4) and are therefore omitted in the plot.

Since aerosol production and westerly transport from North America towards Europe is most effective in the period April–July (e.g., Auvray and Bey, 2005), the sinusoidal curves (thin black lines in Fig. 7) in the control regions have been obtained by only fitting the January-to-March and August-to-December FFAOT values. In addition, to better interpret Fig. 7 results, we show 1) in Fig. 8 two examples of the average FFAOT field in the investigated area (monthly mean of April and July in the period 2002–2007, Fig. 8a and 8b, respectively) and 2) in Fig. 9 the corresponding mean wind fields at 925 mb.

Main outcomes from data in Fig. 7 are as follows: in the three northernmost Atlantic regions (A, B, C) the FFAOT yearly cycle closely follows a sinusoidal behaviour, while in the southernmost regions (G, H, I) a deviation from such regular behaviour is clearly visible from April to July. Figures 8 and 9 reveal this is due to the aerosol production and transport from Northern-Central America. Also, a minor west-to-east gradient (Fig. 7g–i) is observed suggesting that, in this period of the year, the Western Mediterranean target region might still receive a contribution from such transport (thus contributing to the FFAOT values of Fig. 4e). If this is the case, the April-to-July wildfires contributions estimated for the Western Mediterranean (Fig. 6 and Table 2) might be overestimated. Similarly, some deviation from the sinusoidal behaviour is found in control regions D (July) and E (June–July). The FFAOT field (Fig. 8b) indicates this deviation to be still

ACPD
11, 2317–2354, 2011

due to aerosols advected from North America, which, favoured by the high wind speed (Fig. 9b), reach up to that latitudes. In this case a West-to-East gradient is observed (Fig. 7d–f) and the effect is completely lost off the Irish coasts (Fig. 7f). Thus no impact from such transport is expected in the Western Europe region considered in this study. Rather, the AOT (and FFAOT) peak observed over this region in March (Fig. 4b) is due to an increase of the aerosol load over ocean, and namely over the English Channel and the Bay of Biscay (not shown here). The reason for such an aerosol increase in this period of the year is unknown, but this allows excluding it is due to fires (we suspect a contamination from algal blooms in the satellite signal, frequent in this period of the year (e.g., Lampert et al., 2002; Gohin et al., 2003), which is misinterpreted as aerosols by the satellite signal inversion scheme). Again, for this month/region the $FFAOT_{FWTD,2}$ estimate in Fig. 6 is likely more reliable than the corresponding $FFAOT_{FWTD,1}$ one.

Overall, this analysis over the Atlantic control regions points to a negligible contamination of westerly particle transport towards Europe on our results, except for the Western Mediterranean region.

4 Discussion and Conclusions

Wildfires (intended here as open fires of peat and various vegetation including forests, grasslands and agricultural residues) represent an important global source of trace gases and aerosols and may represent an important climatic variable as well as a threat for air quality and, more generally, for the environment.

In the European continent agricultural burning, used to remove crop residues for new planting or clear weeds and brush for grazing, is a common practice, in particular in Eastern Europe and European Russia where the largest fraction of wildland fires occurs. A clear identification of the atmospheric effects of these small-scale fires far from the source region is not straightforward, especially in terms of advected particulate matter. In fact, detection of aged smoke is hampered by the important modifications fires-originated particles undergo during the transport, and, in densely populated regions

ACPD
11, 2317–2354, 2011

such as Europe, by the intricate chemical transformations and mixing with other particles of both anthropogenic and natural origin (e.g., Péré et al., 2009). Numerous studies available in literature reported on the impacts of episodic biomass burning events in Europe, but, to our knowledge, these efforts have not yet led to a comprehensive evaluation of the role these fires play on the aerosol load at the continental scale.

In this study we used long term (2002–2007) remote sensing observation of aerosol optical thickness (AOT) and fires combined with atmospheric transport simulations to start filling this gap. Results clearly show how, over Europe, these fires contribute forming a continent-wide smoky haze. As observed in other areas of the world (e.g., McMeeking et al., 2006; Li et al., 2010), this is likely not only caused by the direct increase of the regional aerosol load, but also via modifications of the chemical/physical properties of existing aerosol particles in downwind areas. Notwithstanding some unavoidable simplifications and assumptions, our results indicate that, in spring and summer, 10 to 30% of the fine fraction aerosol optical thickness (FFAOT) in Europe is related to wildfires emissions. Possible contamination of these results from intercontinental transport of pollution from North America is shown to be almost negligible.

In April, when agricultural fires maximize and atmospheric circulation is most favourable (remember for example the dramatic spread to Central and Northern Europe of the Chernobyl nuclear plume, in April 1986, e.g., Albercel et al., 1988), an evident impact of wildfires is visible over Europe, with maximum contribution to the FFAOT of 20–35% in Central and Eastern Europe, Scandinavia and Central Mediterranean. In August the wildfires contribution to the FFAOT overcomes 25% all over the continent, with the exception of Western Europe. With respect to the summer fires, partly associated to the burning of forest-type vegetation, our analysis suggests a still underrated impact of spring agricultural fires (particularly active in Eastern Europe and ex-USSR countries as Ukraine, Kazakhstan and Russian Federation) on the continental AOT, these thus representing a clear target for mitigation (FAO, 2009).

ACPD
11, 2317–2354, 2011

This finding should be also considered in view of the high potential of Eastern Europe, and particularly Ukraine, in terms of land availability for growing bio-energy feedstocks foreseen for the next 30-years (Fisher et al., 2010), thus representing a source region of renewable energy and greenhouse gas emission reductions. In fact, the European Commission's recent report on the sustainability of biomass (EC, 2010) concluded that where forest or agricultural residues are used for heat and power applications, and as long as the biomass production does not cause any land-use change, the greenhouse gas savings of European feedstocks are generally above 80% compared to the fossil fuel alternative.

Given the proven fingerprints of wildfires in the atmospheric column, an aspect that would also merit further investigation is their relevant contribution in the lowest atmospheric levels, i.e., on the European air quality. In fact, some evidences of an important impact at the ground are available in literature. For example, the effect of agricultural burning was well detectable in long-term aerosol measurement performed at the ground in Crete, Greece (e.g., Sciare et al., 2008). A 20-to-200% increase in $PM_{2.5}$ ground concentrations was estimated by Hodzic et al. (2007) over a large part of Europe during the intense fire season that occurred in summer 2003, particularly in Portugal. Unusually high levels of $PM_{2.5}$ and PM_{10} due to long-range transport of smoke from widespread agricultural burning and forest fires in Western Russia were observed in the UK in September 2002 and May 2006 (Witham and Manning, 2007) and in Finland in April-May 2006 (Saarikoski et al., 2007). More recently, a not negligible contribution to PM values at European high altitude background sites has been attributed to long range transport of biomass burning from the Baltic countries, Byelorussia, Western Russia and Kazakhstan (Salvador et al., 2010). However, as for the AOT observations, these studies are still fragmented in space and time so that a comprehensive assessment of this effect at the European scale is also missing. A very preliminary estimate from our results would suggest a spring and summer contribution of wildfires to monthly-mean PM levels at the ground of about 10 $\mu g/m^3$ (considering a mean wildfires FFAOT of 0.04, e.g., Fig. 6, and assuming a typical mass-to-extinction coefficient

ACPD
11, 2317–2354, 2011

of 4.0 m^2/g (Reid et al., 2005b), we get a total columnar mass of M=0.01 g/m^2, which, if uniformly distributed within a 1000 m-thick atmospheric column, gives the estimated value at the ground of 10 µg/m^3). This contribution would definitely be significant for air quality evaluation purposes, considering the 50 µg/m^3 daily threshold (not to be exceeded more than 35 times per calendar year) established by the current European legislation (Directive 2008/50/EC).

Supplementary material related to this article is available online at: http://www.atmos-chem-phys-discuss.net/11/2317/2011/acpd-11-2317-2011-supplement.pdf.

Acknowledgements. The authors gratefully acknowledge the MODIS and MISR mission scientists and associated NASA personnel for the production of the data used in this research effort and the NOAA Air Resources Laboratory (ARL) for the provision of the HYSPLIT transport and dispersion model used in this publication. The MISR data were obtained from the NASA Langley Research Center Atmospheric Sciences Data Center. MODIS fires count data used in this study were obtained from the NEO web portal as part of the NASA EOS Project Science Office. MODIS FRP data were produced with the Giovanni online data system (NASA GES DISC) under the NASA Northern Eurasia Earth Science Partnership Initiative – NEESPI. The NASA NEESPI Data and Services Center project is supported by NASA HQ through ROSES 2005 NNH05ZDA001N-ACCESS.

References

Acker, J. G. and Leptoukh, G.: Online analysis enhances use of NASA earth science data, Eos, Trans. Am. Geophys. Union, 88(2), 14–17, 2007.

Aculinin, A., Holben, B., Smirnov, A., and Eck, T.: Measurements of aerosol optical properties at the Kishinev site, Moldova, Moldav. J. Phys. Sci., 3(N2), 214–225, 2004.

Ahmed, A. A., Mohamed, A., Ali, A. E., Barakat, A., Abd El-Hady, M., and El-Hussein, A.: Seasonal variations of aerosol residence time in the lower atmospheric boundary layer, J. Environ. Radioactiv., 77, 275–283, 2004.

ACPD
11, 2317–2354, 2011

Albercel A., Martini, D., Strauss, B., and Gross, J.-M.: The Chernobyl accident: modelling of dispersion over Europe of the radioactive plume and comparison with air activity measurements, Atmos. Environ., 22, 2431–2444, 1988.
Amiridis, V., Balis, D. S., Giannakaki, E., Stohl, A., Kazadzis, S., Koukouli, M. E., and Zanis, P.: Optical characteristics of biomass burning aerosols over Southeastern Europe determined from UV-Raman lidar measurements, Atmos. Chem. Phys., 9, 2431–2440, doi:10.5194/acp-9-2431-2009, 2009.
Andreae, M. O. and Merlet, P.: Emission of trace gases and aerosols from biomass burning, Global Biogeochem. Cy., 15, 955–966, 2001.
Arola, A., Lindfors, A., Natunen, A., and Lehtinen, K. E. J.: A case study on biomass burning aerosols: effects on aerosol optical properties and surface radiation levels, Atmos. Chem. Phys., 7, 4257–4266, doi:10.5194/acp-7-4257-2007, 2007.
Auvray, M. and Bey I.: Long-range transport to Europe: Seasonal variations and implications for the European ozone budget, J. Geophys. Res., 110, D11303, doi:10.1029/2004JD005503, 2005.
Balis D. S., Amiridis, V., Zerefos, C., Gerasopoulos, E., Andreae, M., Zanis, P., Kazantzidis, A., Kazadzis, S., and Papayannis, A.: Raman lidar and sunphotometric measurements of aerosol, optical properties over Thessaloniki, Greece during a biomass burning episode, Atmos. Environ., 37, 4529–4538, 2003.
Barnaba, F. and Gobbi, G. P.: Aerosol seasonal variability over the Mediterranean region and relative impact of maritime, continental and Saharan dust particles over the basin from MODIS data in the year 2001, Atmos. Chem. Phys., 4, 2367–2391, doi:10.5194/acp-4-2367-2004, 2004.
Chubarova, N. Y.: Seasonal distribution of aerosol properties over Europe and their impact on UV irradiance, Atmos. Meas. Tech., 2, 593–608, doi:10.5194/amt-2-593-2009, 2009.
d'Almeida, G. A., Koepke, P., and Shettle, E. P.: Atmospheric aerosols: global climatology and radiative characteristics, A. Deepak Pub., Hampton, Va., 561 p., 1991.
Damoah, R., Spichtinger, N., Forster, C., James, P., Mattis, I., Wandinger, U., Beirle, S., Wagner, T., and Stohl, A.: Around the world in 17 days – hemispheric-scale transport of forest fire smoke from Russia in May 2003, Atmos. Chem. Phys., 4, 1311–1321, doi:10.5194/acp-4-1311-2004, 2004.
Diner, D. J., Beckert, J. C., Reilly, T. H., Bruegge, C. J., Conel, J. E., Kahn, R., Martonchik, J. V., Ackerman, T. P., Davies, R., Gerstl, S. A. W., Gordon, H. R., Muller, J.-P., Myneni, R., Sell-

ACPD
11, 2317–2354, 2011

ers, R. J., Pinty, B., and Verstraete, M. M.: Multi-angle Imaging Spectro Radiometer (MISR) description and experiment overview, IEEE Trans. Geosci. Remote Sens., 36(4), 1072–1087, 1998.

Draxler, R. R. and Hess, G. D.: An overview of the HYSPLIT_4 modeling system of trajectories, dispersion, and deposition, Aust. Meteorol. Mag., 47, 295–308, 1998.

EC-European Commission: Report from the Commission to the Council and the European Parliament on sustainability requirements for the use of solid and gaseous biomass sources in electricity, heating and cooling, COM(2010)11, Brussels, 2010.

Edwards, D. P., Emmons, L. K., Hauglustaine, D. A., Chu, D. A., Gille, J. C., Kaufman, Y. J., Petron, G., Yurganov, L. N., Giglio, L., Deeter, M. N., Yudin, V., Ziskin, D. C., Warner, J., Lamarque, J.-F., Francis, G. L., Ho, S. P., Mao, D., Chen, J., Grechko, E. I., and Drummond, J. R.: Observations of carbon monoxide and aerosols from the Terra satellite: Northern Hemisphere variability, J. Geophys. Res., 109, D24202, doi:10.1029/2004JD004727, 2004.

FAO (Food and Agriculture Organization): Forest fires and the law – a guide for national drafters based on the Fire Management Voluntary Guidelines, FAO LEGISLATIVE STUDY 99, Rome, Italy, ISBN:978-92-5-106151-0, 175 pp., 2009.

Fischer, G., Prieler, S., van Velthuizen, H., Berndes, G., Faaij, A., Londo, M., and de Wit, M.: Biofuel production potentials in Europe: sustainable use of cultivated land and pastures, Part II: Land use scenarios, Biomass Bioenerg., 34, 173–187, 2010.

Formenti, P., Boucher, O., Reiner, T., Sprung, D., Meinrat, O. A., Wendisch, M., Wex, H., Kindred, D., Tzortziou, M., Vasaras, A., and Zerefos, C.: STAAARTE-MED 1998 summer airborne measurements over the Aegean Sea, 2, Aerosol scattering and absorption, and radiative calculations, J. Geophys. Res., 107, 4451, doi:10.1029/2001JD001536, 2002.

Generoso, S., Bey, I., Attié, J.-L., and Bréon, F.-M.: A satellite- and model-based assessment of the 2003 Russian fires: Impact on the Arctic region, J. Geophys. Res., 112, D15302, doi:10.1029/2006JD008344, 2007.

Giglio, L., Descloitres, J., Justice, C. O., and Kaufman, Y.: An enhanced contextual fire detection algorithm for MODIS, Remote Sens. Environ., 87, 273–282, 2003.

Giglio, L., Csiszar, I., and Justice, C. O.: Global distribution and seasonality of active fires as observed with the Terra and Aqua Moderate Resolution Imaging Spectroradiometer (MODIS) sensors, J. Geophys. Res., 111, G02016, doi:10.1029/2005JG000142, 2006.

Gohin F., Lampert, L., Guillaud, J.-F., Herbland, A., and Nézan, E.: Satellite and in situ observations of a late winter phytoplankton bloom, in the Northern Bay of Biscay, Cont. Shelf Res.,

ACPD
11, 2317–2354, 2011

23, 1117–1141, 2003.
Hays, M. D., Fine, P. M., Geron, C. D., Kleeman, M. J., and Gullett, B. K.: Open burning of agricultural biomass: physical and chemical properties of particle-phase emissions, Atmos. Environ., 39, 6747–6764, 2005.
Hodzic, A., Madronich, S., Bohn, B., Massie, S., Menut, L., and Wiedinmyer, C.: Wildfire particulate matter in Europe during summer 2003: meso-scale modeling of smoke emissions, transport and radiative effects, Atmos. Chem. Phys., 7, 4043–4064, doi:10.5194/acp-7-4043-2007, 2007.
Holben, B. N., Eck, T. F., Slutsker, I., Tanre, D., Buis, J. P., Setzer, A., Vermote, E., Reagan, J. A., Kaufman, Y. J., Nakajima, T., Lavenu, F., Jankowiak, I., and Smirnov, A.: AERONET – a federated instrument network and data archive for aerosol characterization, Remote Sens. Environ., 66(1), 1–16, 1998.
Huntrieser, H., Heland, J., Schlager, H., Forster, C., Stohl, A., Aufmhoff, H., Arnold, F., Scheel, H. E., Campana, M., Gilge, S., Eixmann, R., and Cooper, O.: Intercontinental air pollution transport from North America to Europe: experimental evidence from airborne measurements and surface observations, J. Geophys. Res., 110, D01305, doi:10.1029/2004JD005045, 2005.
Janhäll, S., Andreae, M. O., and Pöschl, U.: Biomass burning aerosol emissions from vegetation fires: particle number and mass emission factors and size distributions, Atmos. Chem. Phys., 10, 1427–1439, doi:10.5194/acp-10-1427-2010, 2010.
Justice C., Giglio, L., Boschetti, L., Roy, D., Csiszar, I., Morisette, J., and Kaufman, Y.: Modis Fire Products – Algorithm Technical Background Document, 2006, available at: http://modis.gsfc.nasa.gov/data/atbd/atbd_mod14.pdf, last access: 20 January 2011, 2006.
Kasischke, E. S. and Penner, J. E.: Improving global estimates of atmospheric emissions from biomass burning, J. Geophys. Res., 109, D14S01, doi:10.1029/2004JD004972, 2004.
Kahn, R. A., Gaitley, B. J., Garay, M. J., Diner, D. J., Eck, T., Smirnov, A., and Holben, B. N.: MISR aerosol product assessment by comparison with AERONET, J. Geophys. Res., doi:10.1029/2010JD014601, 115, D23209, doi:10.1029/2010JD014601, 2010.
Kaufman, Y. J., Justice, C. O., Flynn, L. P., Kendall, J. D., Prins, E. M., Giglio, L., Ward, D. E., Menzel, W. P., and Setzer, A. W.: Potential global fire monitoring from EOS-MODIS, J. Geophys. Res., 103, 32215–32238, 1998.
Koelemeijer, R. B. A., Homan, C. D., and Matthijsen, J.: Comparison of spatial and temporal variations of aerosol optical thickness and particulate matter over Europe, Atmos. Environ.,

ACPD
11, 2317–2354, 2011

40, 5304–5315, 2006.
Korontzi, S., McCarty, J., Loboda, T., Kumar, S., and Justice, C.: Global distribution of agricultural fires in croplands from 3 years of Moderate Resolution Imaging Spectroradiometer (MODIS) data, Global Biogeochem. Cy., 20, GB2021, doi:10.1029/2005GB002529, 2006.
Lampert, L., Quéguiner, B., Labasque, T., Pichon, A., and Lebreton, N.: Spatial variability of phytoplankton composition and biomass on the eastern continental shelf of the Bay of Biscay (North-east Atlantic Ocean). Evidence for a bloom of *Emiliania huxleyi* (Prymnesiophyceae) in spring 1998, Cont. Shelf Res., 22, 1225–1247, 2002.
Langmann B., Duncan, B., Textor, C., Trentmannd, J., and van der Werf, G.: Vegetation fire emissions and their impact on air pollution and climate, Atmos. Environ., 43, 107–116, 2009.
Li, Q., Jacob, D. J., Park, R., Wang, Y., Heald, C. L., Hudman, R., Yantosca, R. M., Martin, R. V., and Evans, M.: North American pollution outflow and the trapping of convectively lifted pollution by upper-level anticyclone, J. Geophys. Res., 110, D10301, doi:10.1029/2004JD005039, 2005.
Li, W. J., Shao, L. Y., and Buseck, P. R.: Haze types in Beijing and the influence of agricultural biomass burning, Atmos. Chem. Phys., 10, 8119–8130, doi:10.5194/acp-10-8119-2010, 2010.
Marmer, E., Langmann, B., Fagerli, H., and Vestreng, V.: Direct shortwave radiative forcing of sulfate aerosol over Europe from 1900 to 2000, J. Geophys. Res., 112, D23S17, doi:10.1029/2006JD008037, 2007.
Martonchik, J. V., Kahn, R. A., and Diner, D. J.: Retrieval of aerosol properties over land using MISR observations, in: Satellite Aerosol Remote Sensing Over Land, edited by: Kokhanovsky, A. A. and de Leeuw, G., Springer Praxis Books, Berlin, 267–293, doi:10.1007/978-3-540-69397-0_9, 2009.
McMeeking, G. R., Kreidenweis, S. M., Lunden, M., Carrillo, J., Carrico, C. M., Lee, T., Herckes, P., Engling, G., Day, D. E., Hand, J., Brown, N., Malm, W. C., and Collett, J. L.: Smoke-impacted regional haze in California during the summer of 2002, Agr. Forest Meteorol., 137, 25–42, 2006.
Menut, L. and Bessagnet, B.: Atmospheric composition forecasting in Europe, Ann. Geophys., 28, 61–74, doi:10.5194/angeo-28-61-2010, 2010.
Mehta, A. V. and Yang, S.: Precipitation climatology over Mediterranean Basin from ten years of TRMM measurements, Adv. Geosci., 17, 87–91, doi:10.5194/adgeo-17-87-2008, 2008.
Mollicone D., Eva, H. D., and Achard, F.: Human role in Russian wild fires, Nature, 440, 436–

ACPD
11, 2317–2354, 2011

437, doi:10.1038/440436a, 2006.
Moulin, C., Lambert, C. E., Dayan, U., Masson, V., Ramonet, M., Bousquet, P., Legrand, M., Balkanski, Y. J., Guelle, W., Marticorena, B., Bergametti, G., and Dulac, F.: Satellite climatology of African dust transport in the Mediterranean atmosphere, J. Geophys. Res., 103, 13137–13144, 1998.
Muller, D., Mattis, I., Wandinger, U., Ansmann, A., Althausen, D., and Stohl, A.: Raman lidar observations of aged Siberian and Canadian forest fire smoke in the free troposphere over Germany in 2003: microphysical particle characterization, J. Geophys. Res., 110, D17201, doi:10.1029/2004JD005756, 2005.
Niemi, J. V., Tervahattu, H., Vehkamäki, H., Martikainen, J., Laakso, L., Kulmala, M., Aarnio, P., Koskentalo, T., Sillanpää, M., and Makkonen, U.: Characterization of aerosol particle episodes in Finland caused by wildfires in Eastern Europe, Atmos. Chem. Phys., 5, 2299–2310, doi:10.5194/acp-5-2299-2005, 2005.
Pace, G., Meloni, D., and di Sarra, A.: Forest fire aerosol over the Mediterranean Basin during summer 2003, J. Geophys. Res., 110, D21202. doi:10.1029/2005JD005986, 2005.
Papadimas, C. D., Hatzianastassiou, N., Mihalopoulos, N., Querol, X., and Vardavas, I.: Spatial and temporal variability in aerosol properties over the Mediterranean Basin based on 6-year (2000–2006) MODIS data, J. Geophys. Res., 113, D11205, doi:10.1029/2007JD009189, 2008.
Papayannis, A., Amiridis, V., Mona, L., Tsaknakis, G., Balis, D., Bosenberg, J., Chaikovski, A., De Tomasi, F., Grigorov, I., Mattis, I., Mitev, V., Muller, D., Nickovic, S., Perez, C., Pietruczuk, A., Pisani, G., Ravetta, F., Rizi, V., Sicard, M., Trickl, T., Wiegner, M., Gerding, M., Mamouri, R. E., D'Amico, G., and Pappalardo, G.: Systematic lidar observations of Saharan dust over Europe in the frame of EARLINET (2000–2002), J. Geophys. Res., 113, D10204, doi:10.1029/2007JD009028, 2008.
Papastefanou, C.: Residence time of tropospheric aerosols in association with radioactive nuclides, Appl. Radiat. Isotopes, 64, 93–100, 2006.
Penkett, S. A., Law, K., Platt, U., and Volz-Thomas, A.: European export of particulates and ozone by long-range transport – overview of subproject EXPORT-E2, in: Towards Cleaner Air for Europe – Science, Tools and Applications – Part 2. Overviews from the Final Reports of the EUROTRAC-2 Subprojects, edited by: Midgley, P. M. and Reuther, M., M. Margraf Verlag, Weikersheim (DE), ISBN:3-8236-1391-X, 99–118, 2003.
Péré, J. C., Mallet, M., Bessagnet, B., and Pont, V.: Evidence of the aerosol core-shell mixing

ACPD
11, 2317–2354, 2011

state over Europe during the heat wave of summer 2003 by using CHIMERE simulations and AERONET inversions, Geophys. Res. Lett., 36, L09807, doi:10.1029/2009GL037334, 2009.
Reid, J. S., Koppmann, R., Eck, T. F., and Eleuterio, D. P.: A review of biomass burning emissions part II: intensive physical properties of biomass burning particles, Atmos. Chem. Phys., 5, 799–825, doi:10.5194/acp-5-799-2005, 2005a.
Reid, J. S., Eck, T. F., Christopher, S. A., Koppmann, R., Dubovik, O., Eleuterio, D. P., Holben, B. N., Reid, E. A., and Zhang, J.: A review of biomass burning emissions part III: intensive optical properties of biomass burning particles, Atmos. Chem. Phys., 5, 827–849, doi:10.5194/acp-5-827-2005, 2005b.
Rangarajan, C.: A study of the mean residence time of the natural radioactive aerosols in the planetary boundary layer, J. Environ. Radioactiv., 15, 193–206, 1992.
Saarikoski, S., Sillanpaa, M., Sofiev, M., Timonen, H., Saarnio, K., Teinila, K., Karppinen, A., Kukkonen, J., and Hillamo, R.: Chemical composition of aerosols during a major biomass burning episode over Northern Europe in spring 2006: experimental and modelling assessments, Atmos. Environ., 41, 3577–3589, 2007.
Saarnio, K., Aurela, M., Timonen, H., Saarikoski, S., Teinilä, K., Mäkelä, T., Sofiev, M., Koskinen, J., Aalto, P. P., Kulmala, M., Kukkonen, J., and Hillamo, R.: Chemical composition of fine particles in fresh smoke plumes from boreal wild-land fires in Europe, Sci. Total Environ., 408, 12, 2527–2542, 2010.
Salvador, P., Artíñano, B., Pio, C., Afonso, J., Legrand, M., Puxbaum, H., and Hammer, S.: Evaluation of aerosol sources at European high altitude background sites with trajectory statistical methods, Atmos. Environ., 44, 2316–2329, 2010.
Sicard, M., Rocadenbosch, F., Reba, M. N. M., Comerón, A., Tomás, S., García-Vízcaino, D., Batet, O., Barrios, R., Kumar, D., and Baldasano, J. M.: Seasonal variability of aerosol optical properties observed by means of a Raman lidar at an EARLINET site over Northeastern Spain, Atmos. Chem. Phys., 11, 175–190, doi:10.5194/acp-11-175-2011, 2011.
Sciare, J., Oikonomou, K., Favez, O., Liakakou, E., Markaki, Z., Cachier, H., and Mihalopoulos, N.: Long-term measurements of carbonaceous aerosols in the Eastern Mediterranean: evidence of long-range transport of biomass burning, Atmos. Chem. Phys., 8, 5551–5563, doi:10.5194/acp-8-5551-2008, 2008.
Treffeisen, R., Tunved, P., Ström, J., Herber, A., Bareiss, J., Helbig, A., Stone, R. S., Hoyningen-Huene, W., Krejci, R., Stohl, A., and Neuber, R.: Arctic smoke – aerosol characteristics during a record smoke event in the European Arctic and its radiative impact, Atmos. Chem.

ACPD
11, 2317–2354, 2011

Phys., 7, 3035-3053, doi:10.5194/acp-7-3035-2007, 2007.
Tegen, I., Koch, D., Lacis, A. L., and Sato, M.: Trends in tropospheric aerosol loads and corresponding impact on direct radiative forcing between 1950 and 1990: a model study, J. Geophys. Res., 105, 26971–26989, 2000.
Warneke, C., Froyd, K. D., Brioude, J., Bahreini, R., Brock, C. A., Cozic, J., de Gouw, J. A., Fahey, D. W., Ferrare, R., Holloway, J. S., Middlebrook, A. M., Miller, L., Montzka, S., Schwarz, J. P., Sodemann, H., Spackman, J. R., and Stohl, A.: An important contribution to springtime Arctic aerosol from biomass burning in Russia, Geophys. Res. Lett., 37, L01801, doi:10.1029/2009GL041816, 2010.
Wiedinmyer, C., Quayle, B., Geron, C., Belote, A., McKenzie, D., Zhang, X., O'Neill, S., Klos, K., and Wynne, K. K.: Estimating emissions from fires in North America for air quality modelling, Atmos. Environ., 40, 3419–3432, 2006.
Witham, C. and Manning, A.: Impacts of Russian biomass burning on UK air quality, Atmos. Environ., 41, 8075–8090, 2007.
Wooster, M. J., Roberts, G., and Perry, G. L. W.: Retrieval of biomass combustion rates and totals from fire radiative power observations: FRP derivation and calibration relationships between biomass consumption and fire radiative energy release, J. Geophys. Res., 110, D24311, doi:10.1029/2005JD006318, 2005
Yu, H., Dickinson, R. E., Chin, M., Kaufman, Y. J., Holben, B. N., Geogdzhayev, I. V., and Mishchenko, M. I.: Annual cycle of global distributions of aerosol optical depth from integration of MODIS retrievals and GOCART model simulations, J. Geophys. Res., 108(D3), 4128, doi:10.1029/2002JD002717, 2003.

ACPD
11, 2317–2354, 2011

Table 1. Correction factors derived (Eq. 7) for the seven regions addressed in this study and used to convert FWTD values into FFAOT values (Eq. 6).

Target region	CF ($\times 1^{10}$)
Western Med (WMed)	2.6±1.7
Central Med (CMed)	2.7±1.3
Turkey (TUR)	3.2±1.7
Western Europe (WEU)	3.1±5.5
Central Europe (CEU)	3.4±1.7
Eastern Europe (EEU)	2.7±1.4
Scandinavia (SCA)	7.4±5.9

ACPD
11, 2317–2354, 2011

Table 2. Monthly and regional values (±1 st. dev.) of the estimated wildfires contribution to the FFAOT, $FFAOT_{WF\_mean}$, and (in parenthesis) relative percentage to the total FFAOT.

Region	Month											
	J	F	M	A	M	J	J	A	S	O	N	D
SCA	−0.0006 ±0.0019 (−2±7)	0.0016 ±0.0003 (4±1)	0.014 ±0.003 (22±4)	0.033 ±0.004 (35±4)	0.02 ±0.01 (21±12)	0.005 ±0.007 (7±11)	0.012 ±0.008 (17±12)	0.024 ±0.002 (29±2)	0.0163 ±0.0002 (25.8±0.2)	0.003 ±0.008 (10±23)	0.001 ±0.001 (5±5)	0.0005 ±0.0004 (2±1)
WEU	−0.001 ±0.003 (−3±7)	0.002 ±0.002 (4±3)	0.002 ±0.002 (18±16)	0.014 ±0.006 (14±6)	0.001 ±0.003 (1±3)	0.001 ±0.002 (1±2)	0.002 ±0.007 (3±7)	0.001 ±0.009 (1±10)	0.006 ±0.001 (8±1)	0.0043 ±0.0003 (7±1)	0.0013 ±0.0005 (3±1)	−0.0003 ±0.0010 (−1±2)
CEU	−0.003 ±0.001 (1±2)	0.0018 ±0.0006 (3±1)	0.021 ±0.009 (21±9)	0.035 ±0.006 (27±5)	0.009 ±0.001 (8±1)	0.004 ±0.006 (3±5)	0.022 ±0.006 (18±5)	0.032 ±0.004 (25±3)	0.0194 ±0.0005 (21±1)	0.006 ±0.006 (11±10)	0.0022 ±0.0004 (5±1)	−0.001 ±0.002 (−2±7)
EEU	0.001 ±0.002 (0±3)	0.002 ±0.002 (4±3)	0.013 ±0.006 (16±7)	0.04 ±0.01 (30±10)	0.016 ±0.003 (14±2)	0.004 ±0.006 (4±6)	0.032 ±0.006 (24±4)	0.035 ±0.005 (28±4)	0.024 ±0.002 (25±3)	0.007 ±0.007 (12±11)	0.002 ±0.001 (4±3)	0.000 ±0.001 (0±3)
WMD	−0.0002 ±0.0037 (0±8)	0.0034 ±0.0007 (6±1)	0.007 ±0.002 (10±3)	0.008 ±0.008 (10±10)	0.003 ±0.006 (4±7)	0.013 ±0.007 (13±7)	0.018 ±0.004 (19±4)	0.025 ±0.003 (25±3)	0.0164 ±0.0005 (21±1)	0.0111 ±0.0004 (18±1)	0.002 ±0.001 (5±3)	0.0002 ±0.0015 (1±4)
CMD	0.001 ±0.003 (2±5)	0.003 ±0.001 (4±2)	0.018 ±0.003 (19±3)	0.027 ±0.006 (22±5)	0.006 ±0.009 (5±8)	0.015 ±0.006 (12±4)	0.031 ±0.005 (23±4)	0.035 ±0.003 (26±2)	0.021 ±0.004 (19±4)	0.009 ±0.008 (11±10)	0.003 ±0.001 (4±2)	−0.0004 ±0.0028 (−1±5)
TUR	−0.001 ±0.004 (0±7)	0.0046 ±0.0002 (5.5±0.2)	0.014 ±0.008 (14±9)	0.021 ±0.006 (18±5)	0.01 ±0.01 (6±10)	0.017 ±0.008 (14±7)	0.036 ±0.002 (27±1)	0.044 ±0.005 (34±4)	0.029 ±0.001 (29±1)	0.016 ±0.004 (21±5)	0.004 ±0.001 (6±2)	−0.0004 ±0.0030 (0±5)

ACPD
11, 2317–2354, 2011

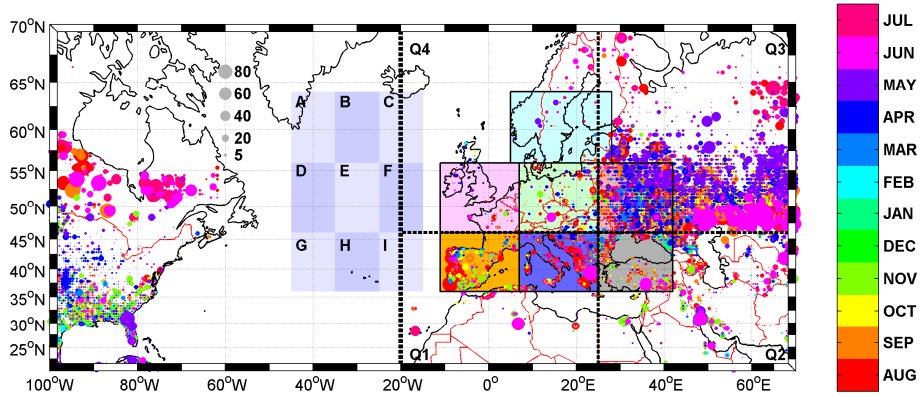

Fig. 1. Monthly mean Fire Counts (FC) from MODIS Terra data in the period 2002–2007 (circles). The size and colour of the circles refer, respectively, to the fire count value (FC/1000 km^2/day) and month of the year (see relevant legends). The map also shows: (i) the seven target regions addressed in this study and namely Scandinavia (cyan), Western Europe (magenta), Central Europe (green), Eastern Europe (red), Western Mediterranean (orange), Central Mediterranean (blue) and Turkey (gray); (ii) the whole region considered for the FWTD computations (20° W–70° E; 20° N–70° N, delimited by the thick dotted line) and its division into four quadrants Q1-to-Q4 (thin dashed line-delimited areas); (iii) the seven Atlantic control regions considered in the study (violet areas, labelled A to I).

ACPD
11, 2317–2354, 2011

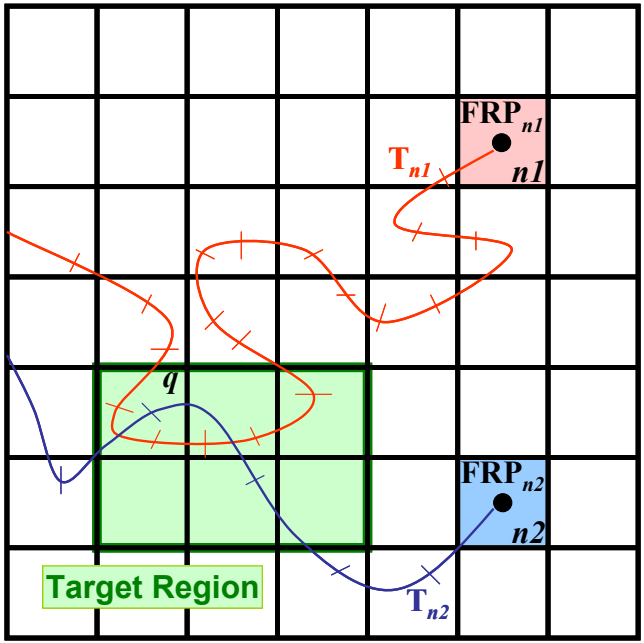

Fig. 2. Schematic of the procedure used to build the FWTD quantity (2.5°-resolution) used in this study (see Sect. 2.3.1 for details). The subscript *n* identifies the starting cell (associated to a fire count value, FC_n>25 fire counts/1000 km^2/day and to a fire radiative power value FRP_n); *q* is the target cell. A single, 10-day forward trajectory T_n starts from the centre of cell *n* in each day of the month at 10:30 LT. Trajectories are resolved hourly (here represented as trajectory segments). Each target cell *q* receives contributions from each starting cell *n*, leading to build up the monthly resolved FWTD field (e.g., Fig. 3). FWTD averages over a given target region (here represented by the green area) are also obtained from this fields (e.g., Fig. 4).

ACPD
11, 2317–2354, 2011

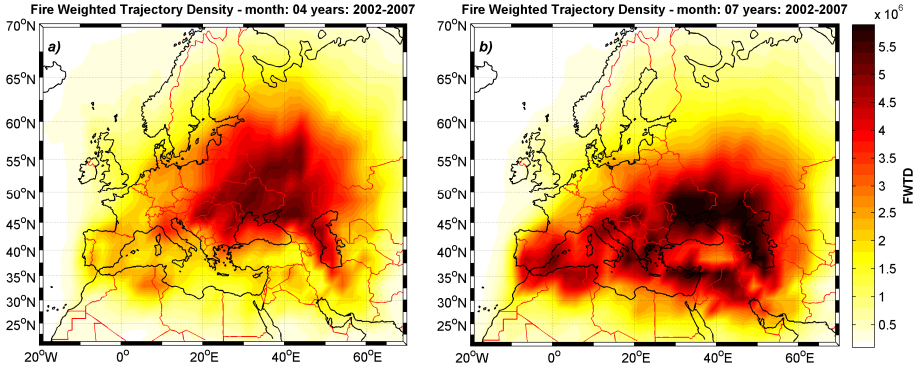

Fig. 3. FWTD fields obtained for the months of April **(a)** and July **(b)** as average over the 2002–2007 period.

ACPD
11, 2317–2354, 2011

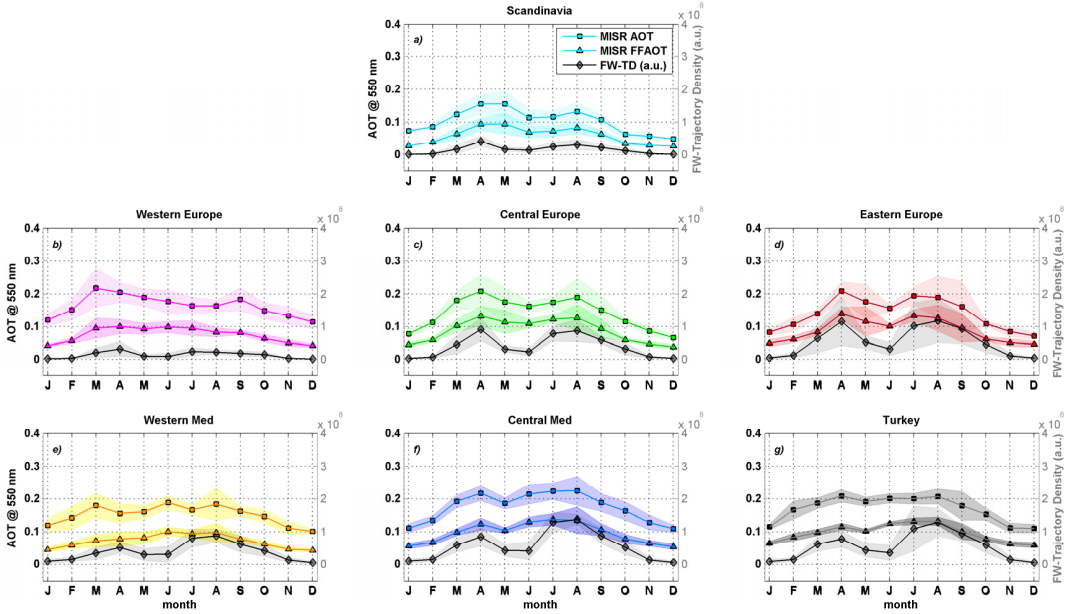

Fig. 4. Monthly mean AOT (squares) and FFAOT (triangles) derived from MISR data in the period 2002–2007 in the seven target regions addressed in this study (panels **a**–**g**), and corresponding FWTD values (diamonds, right axis) computed coupling MODIS fires data with forward trajectories computations (see Sect. 2.3.1 for details). For each variable, shaded areas indicate ±1 standard deviation.

ACPD
11, 2317–2354, 2011

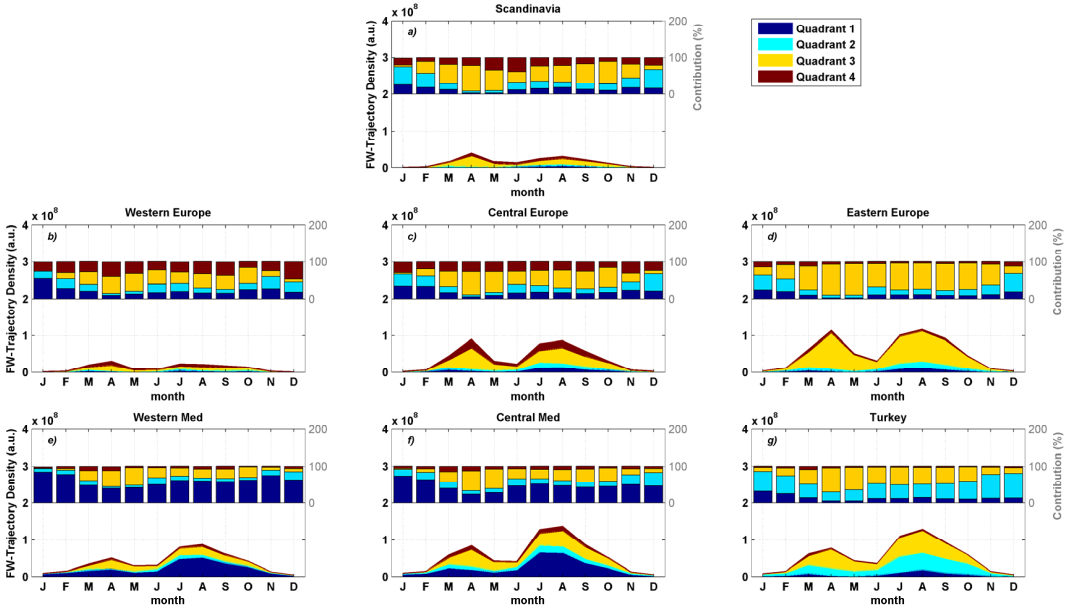

Fig. 5. Absolute (left axis) and percent (histograms, right axis) contribution of the four quadrants Q1–Q4 (Fig. 1) to the FWTD derived for the seven target regions addressed in this study.

ACPD
11, 2317–2354, 2011

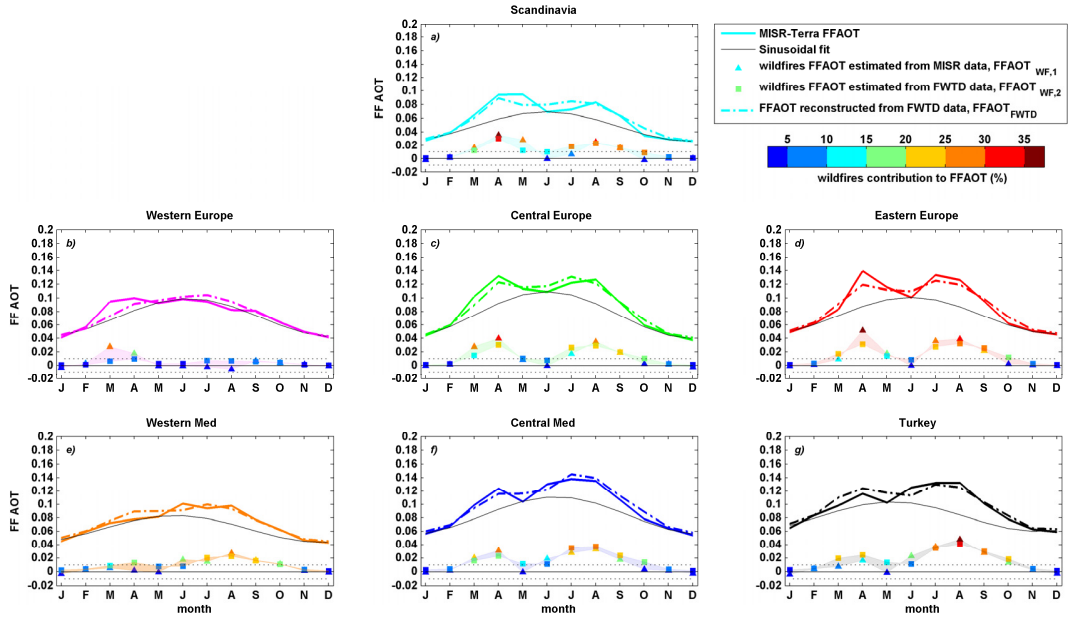

Fig. 6. Each panel (**a**–**g**, referring to one of the seven target regions addressed in this study) shows: (i) the monthly mean FFAOT as measured by MISR (thick coloured line); (ii) the monthly mean wildfires contributions to the FFAOT as estimated from the MISR FFAOT data ($FFAOT_{WF,1}$, coloured triangles) and from the FWTD computations ($FFAOT_{WF,2}$, coloured squares, the symbol colour indicating the relative percentage with respect to the total FFAOT, see colour bar); (iii) the sinusoidal fit, $FFAOT_{RB}$, used to derive $FFAOT_{WF,1}$ (thin black line); and (iv) the total FFAOT as reconstructed from $FFAOT_{WF,2}$ plus the sinusoidal fit, $FFAOT_{RB}$ (thick dash dotted line, see Sect. 3.1 for details).

ACPD
11, 2317–2354, 2011

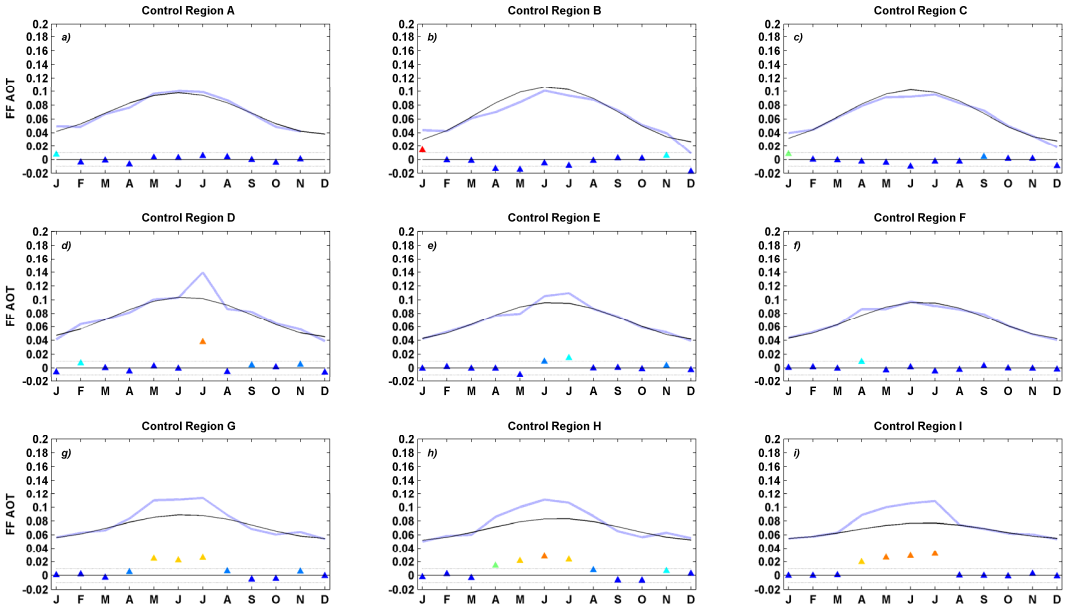

Fig. 7. Each panel (**a**–**i**, referring to one of the nine "control regions" A–I of Fig. 1) shows the monthly mean FFAOT as measured by MISR (thick gray line) and the relevant sinusoidal fit, $FFAOT_{RB}$ (thin black line). Coloured triangles represent the difference $FFAOT - FFAOT_{RB}$ (the colour code indicating the $(FFAOT - FFAOT_{RB})/FFAOT$ percentage, as in Fig. 6).

ACPD
11, 2317–2354, 2011

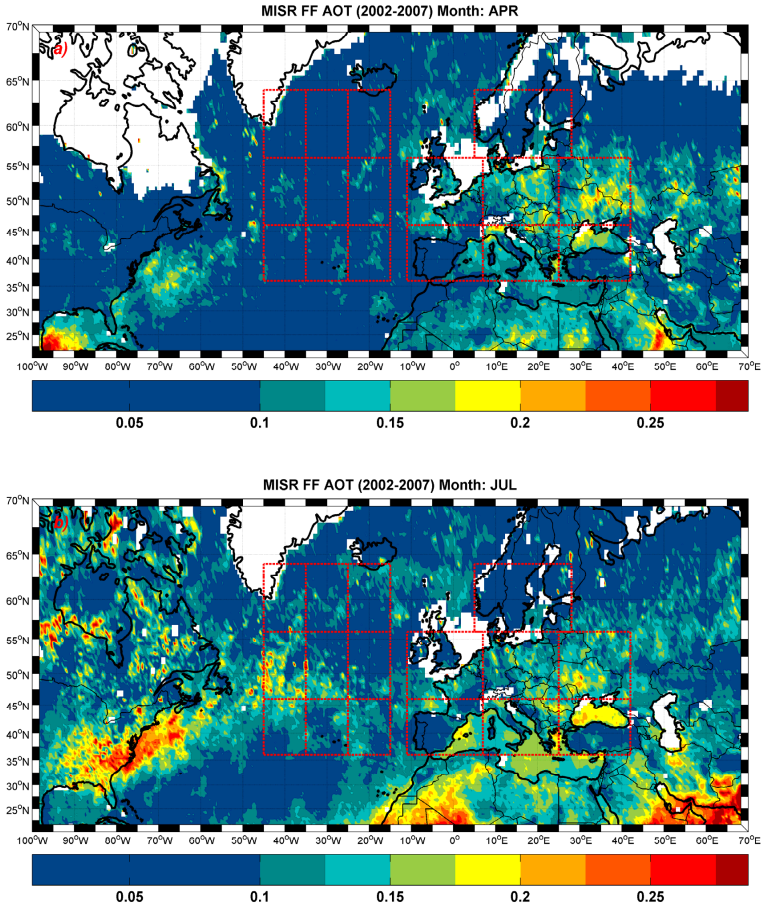

Fig. 8. Monthly mean (years 2002–2007) Fine Fraction Aerosol Optical Thickness (FFAOT) as measured by MISR in April **(a)** and July **(b)**. The seven target European regions and the nine Atlantic control regions are also indicated (red dashed lines).

ACPD
11, 2317–2354, 2011

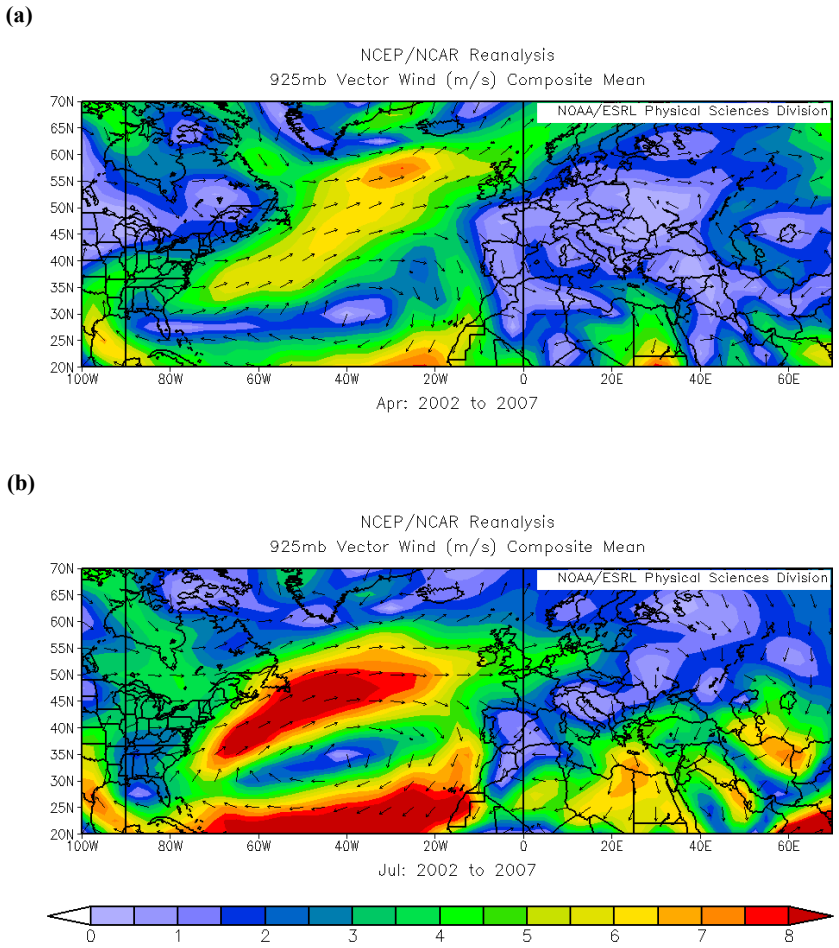

Fig. 9. Monthly mean (2002–2007) wind field at 925 mb in April **(a)** and July **(b)** as derived from NCEP/NCAR reanalysis.

ACPD
11, 2317–2354, 2011